Contribution from the Department of Chemistry, University of Florence, Florence, Italy, Departement de Recherche Fondamentale (UA CNRS 1194), Centre d'Etudes Nucleaires de Grenoble, Grenoble, France, and Service National des Champs Intenses, CNRS, Grenoble, France

One-Dimensional Antiferromagnetism in a Linear Chain Containing Zinc(II) and a Nitronyl Nitroxide

A. Caneschi,[1a] D. Gatteschi,*[,1a] R. Sessoli,[1a] C. I. Cabello,[1a,d] P. Rey,[1b] A. L. Barra,[1c] and L. C. Brunel[1c]

Received August 3, 1990

A compound of formula $Zn(hfac)_2(NIT\text{-}i\text{-}Pr)(H_2O)$, where hfac = hexafluoroacetylacetonate and NIT-*i*-Pr = 2-isopropyl-4,4,5,5-tetramethylimidazoline-1-oxyl 3-oxide, was synthesized. The X-ray analysis shows that it crystallizes in the $P2_1/n$ space group with a = 13.917 (4), Å, b = 13.475 (3), Å, c = 15.885 (9) Å, β = 99.10 (3)°, and Z = 4. The structure consists of discrete molecules in which the zinc ions are octahedrally coordinated by the oxygens of the hfac molecules, an oxygen of the radical, and that of the water molecule. The hydrogen bond between the water molecule and the uncoordinated oxygen of the radical of an adjacent unit generates a chain structure along the b axis. The magnetic susceptibility and the EPR spectra support the description of the system as a typical one-dimensional Heisenberg antiferromagnet. The exchange-coupling constant, J = 12.2 cm^{-1}, has been evaluated from the magnetic data and is attributed to the short contact (3.45 Å) between the NO groups of adjacent radicals. The single-crystal EPR spectra show the angular behavior of the line width and line shape typical of one-dimensional antiferromagnets. Moreover, EPR spectra at high frequency (248 GHz) show the anisotropy effects generated by short-range order, characteristic of one-dimensional systems, which cannot be detected in standard EPR experiments.

Introduction

Nitronyl nitroxides 2-R-4,4,5,5-tetramethylimidazoline-1-oxyl 3-oxide, NITR, are stable organic radicals that can bind to transition-metal ions yielding a large number of different magnetic materials.[2] So for instance when they bind to paramagnetic metal ions, they can form ferrimagnetic rings,[3] one-dimensional ferro- and ferrimagnets,[4-7] and also two-dimensional materials.[8]

When they bind to diamagnetic metal ions, they can form magnetic materials interacting between themselves, and in fact we found that $Y(hfac)_3NITEt$ behaves as a one-dimensional Heisenberg antiferromagnet, with typical behavior that is efficiently monitored by EPR spectroscopy.[9]

We have now found that $Zn(hfac)_2(NIT\text{-}i\text{-}Pr)(H_2O)$ is also a one-dimensional Heisenberg antiferromagnetic even if the exchange pathway is substantially different from that observed in $Y(hfac)_3NITEt$. We wish to report here the X-ray crystal structure and the magnetic properties; in particular we want to show how millimeter range wavelength EPR spectroscopy can provide useful information at low temperature, which cannot be obtained in conventional EPR experiments.

Experimental Section

Synthesis. $Zn(hfac)_2{\cdot}2H_2O$ was obtained by mixing stoichiometric amounts of $Zn(CH_3COO)_2$ and hexafluoroacetylacetone in water. The NIT-*i*-Pr radical was prepared as previously described.[10,11] To 0.5 mmol of $Zn(hfac)_2{\cdot}2H_2O$ dissolved in 60 mL of hot *n*-heptane was added 0.5 mmol of NIT-*i*-Pr radical. The red solution was allowed to stay at room temperature for 1 day and then stored for another 1 day at −5 °C.

Table I. Crystal Data and Experimental Parameters for $Zn(hfac)_2(NITiPr)(H_2O)$

formula	$C_{20}F_{12}H_{23}N_2O_7Zn$	fw	696.75
cryst syst	monoclinic	space group	$P2_1/n$
a	13.917 (4) Å	b	13.475 (3) Å
c	15.885 (9) Å	β	99.10 (3)°
λ	0.7107 Å	density	1.569 g cm^{-3}
V	2941.4	μ	9.30 cm^{-1}
Z	4	temp	22 °C
$R(F_o)$	0.0775	$R_w(F_o)$	0.0815

Well-shaped red crystals suitable for X-ray structure determination and EPR single-crystal measurements were obtained, which were satisfactorily analyzed for $Zn(hfac)_2(NIT\text{-}i\text{-}Pr)(H_2O)$.

Anal. Calcd for $C_{20}F_{12}H_{23}N_2O_7Zn$: C, 34.49; H, 3.32; N, 4.02. Found: C, 34.38; H, 3.24; N, 3.95.

X-ray Data Collection and Structure Solution. X-ray data for $Zn(hfac)_2(NIT\text{-}i\text{-}Pr)(H_2O)$ were collected by mounting a crystal of approximately 0.25 × 0.25 × 0.15 mm on an Enraf-Nonius CAD4 four-circle diffractometer equipped with a Mo Kα X-ray tube and a graphite monochromator. The crystals have the shape of a platelet with the faces (±2,0,±1) largely developed. Crystal and experimental data are given in Table SI (supplementary material) of which Table I is an abbreviated form.

Accurate cell parameters were determined by 22 machine-centered relfections with $8° \le \theta \le 15°$. Two reflections were used as intensity and orientation standards and measured every 160 min during the data collection. Data were corrected for Lorentz and polarization effects but not for absorption.

The structure was solved by conventional methods with the SHELX-76 package.[12] The systematic absences are only compatible with the $P2_1/n$ space group. The position of the zinc atom was determined by a Patterson map; the positions of the other non-hydrogen atoms were found by successive Fourier and difference Fourier synthesis. Some difficulties were met in the refinement procedure due to disorder present in the CF_3 groups of one hexafluoroacetylacetonate moiety. Several unsuccessful attempts were made to find a model group with fractional site occupation factors attributed to the several spots present in the difference Fourier map in positions suitable for fluorine atoms. No better results were obtained by refining the CF_3 groups as rigid groups.

The least-squares procedure converged with an R value of 0.077 and R_w value of 0.081. In the final refinements all the hydrogen atoms were included in fixed and idealized positions. In the final stage of refinement peaks of intensity less than 0.7 e/Å^3 appeared in the Fourier difference map close to the fluorine atoms. Final atomic coordinates are given in Table II.

Magnetic Experiments and EPR Spectra. The magnetic susceptibility of a powdered sample in the range 5-300 K was measured with a DSM5

(1) (a) University of Florence. (b) Centre d'Etudes Nucleaires. (c) Service National de Champs Intenses. (d) Research Career member of Comision de Investigaciones Cientificas, PBA, Argentina.
(2) Caneschi, A.; Gatteschi, D.; Rey, P.; Sessoli, R. *Acc. Chem. Res.* **1989**, *22*, 392.
(3) Caneschi, A.; Gatteschi, D.; Laugier, J.; Rey, P.; Sessoli, R.; Zanchini, C. *J. Am. Chem. Soc.* **1988**, *110*, 2795.
(4) Caneschi, A.; Gatteschi, D.; Laugier, J.; Rey, P. *J. Am. Chem. Soc.* **1987**, *109*, 2191.
(5) Cabello, C. I.; Caneschi, A.; Carlin, R. L.; Gatteschi, D.; Rey, P.; Sessoli, R. *Inorg. Chem.* **1990**, *29*, 2582.
(6) Caneschi, A.; Gatteschi, D.; Renard, J.-P.; Rey, P.; Sessoli, R. *Inorg. Chem.* **1989**, *28*, 1976. Caneschi, A.; Gatteschi, D.; Rey, P.; Sessoli, R. *Inorg. Chem.* **1988**, *27*, 1756.
(7) Caneschi, A.; Gatteschi, D.; Renard, J.-P.; Rey, P.; Sessoli, R. *Inorg. Chem.* **1989**, *28*, 2940.
(8) Caneschi, A.; Gatteschi, D.; Renard, J.-P.; Rey, P.; Sessoli, R. *J. Am. Chem. Soc.* **1989**, *111*, 785. Caneschi, A.; Gatteschi, D.; Melandri, M. C.; Rey, P.; Sessoli, R. *Inorg. Chem.* **1990**, *29*, 4228.
(9) Benelli, C.; Caneschi, A.; Gatteschi, D.; Pardi, L.; Rey, P. *Inorg. Chem.* **1989**, *28*, 3230.
(10) Lamchen, M.; Wittag, T. W. *J. Chem. Soc.* **1966**, 2300.
(11) Ullman, E. F.; Call, L.; Osiecky, J. H. *J. Org. Chem.* **1970**, *35*, 3623.
(12) Sheldrick, G. SHELX 76 Computing Program. University of Cambridge, Cambridge, England, 1976. Atomic scattering factors were from: Cromer, D. T.; Liberman, D. J. *J. Chem. Phys.* **1970**, *53*, 1891.

0020-1669/91/1330-1882$02.50/0

Table II. Positional Parameters (×10⁴) and Isotropic Thermal Factors (Å × 10³) for $Zn(hfac)_2(NITiPr)(H_2O)$[a]

	x/a	y/b	z/c	U_{iso}[b]
Zn	4576 (1)	879 (1)	1297 (1)	40
O1	5273 (5)	435 (5)	2480 (4)	51
O2	5990 (5)	864 (5)	923 (4)	47
O3	3997 (5)	1334 (5)	69 (4)	47
O4	4793 (6)	2377 (5)	1588 (4)	63
O5	4228 (4)	-531 (5)	903 (4)	42
O6	3258 (5)	855 (5)	1799 (5)	56
O7	2165 (8)	3335 (7)	3417 (6)	101
N1	2745 (6)	1592 (6)	2027 (5)	49
N2	2211 (7)	2751 (7)	2783 (6)	64
C1	2956 (8)	2083 (9)	2763 (7)	59
C2	1521 (10)	2790 (10)	1970 (9)	74
C3	1776 (9)	1803 (9)	1533 (8)	64
C4	1815 (13)	3727 (11)	1520 (10)	111
C5	500 (11)	2937 (14)	2105 (11)	131
C6	1133 (12)	969 (12)	1670 (14)	131
C7	1835 (10)	1929 (13)	578 (8)	109
C8	3759 (12)	1913 (12)	3450 (9)	94
C9	3415 (16)	1442 (13)	4238 (9)	154
C10	4358 (13)	2815 (16)	3709 (11)	138
C11	6159 (8)	464 (8)	2753 (7)	51
C12	6917 (8)	682 (8)	2320 (7)	59
C13	6757 (8)	844 (8)	1429 (7)	51
C14	6427 (11)	202 (12)	3686 (8)	74
C15	7650 (13)	976 (22)	1036 (10)	143
C16	4106 (8)	2176 (9)	-228 (7)	55
C17	4496 (9)	3009 (10)	177 (8)	74
C18	4847 (9)	3047 (10)	1041 (9)	71
C19	3659 (12)	2251 (11)	-1161 (8)	78
C20	5248 (22)	4038 (16)	1416 (15)	131
F1	7277 (8)	397 (10)	4054 (5)	162
F2	6381 (13)	-724 (10)	3802 (7)	217
F3	5871 (10)	540 (15)	4125 (5)	259
F4	7674 (8)	715 (16)	327 (8)	203
F5	8452 (7)	932 (20)	1476 (8)	250
F6	7747 (16)	1899 (15)	880 (17)	304
F7	3819 (7)	1519 (6)	-1639 (4)	102
F8	3890 (8)	3049 (7)	-1546 (5)	123
F9	2666 (8)	2323 (9)	-1237 (6)	135
F10	5585 (14)	4579 (10)	898 (9)	224
F11	5935 (16)	3927 (12)	2014 (12)	259
F12	4625 (16)	4499 (13)	1741 (19)	320

[a] Standard deviations in the last digit are in parentheses. [b] $U_{iso} = {}^1/_3\sum_i\sum_j U_{ij}a_i^*a_j^*a_ia_j$.

magnetometer equipped with a Bruker BE15 electromagnet and an Oxford Instruments CF1200S continuous-flow cryostat at a field strength of 1.2 T. The diamagnetic contribution was evaluated by using Pascal's constants.

EPR spectra of powder samples and single crystals were recorded on a Varian E9 spectrometer operating at X- and Q-band frequencies. A single crystal was mounted on a sample holder that allowed rotation along the orthogonal axes $a^* = b \times c$, b, and c. Temperatures in the range 4.2–300 K were obtained with an Oxford Instruments ESR9 continuous-flow cryostat.

High-field EPR experiments were performed with a homemade spectrometer.[13] An optically (CO_2 laser) pumped far-infrared waveguide laser is used as the radiation source and can provide emission lines at several wavelengths between 0.5 and 2 mm. The absorption of the far-IR radiation through the sample was recorded by a germanium composite bolometer working at low temperature ($T \simeq 1.6$ K). The main magnetic field is provided by a Cryogenic Consultant superconducting magnet, working up to 13 T at 2.2 K with an homogeneity of 5×10^{-5} T within 1 cm³. An additional coil superimposes an alternating field with a frequency of 70 Hz. Thus, the derivative of the signal is recorded by a lock-in.

Results

Crystal Structure. The structure of $Zn(hfac)_2(NIT\text{-}i\text{-}Pr)(H_2O)$ consists of discrete octahedral molecules with the zinc octahedrally coordinated by two hfac ligands and by the oxygen atoms of NIT-*i*-Pr and H_2O in a cis position. A view of the molecular structure is shown in Figure 1. The distortions from a regular octahedron around the zinc atoms are rather small, as shown in Tables III and IV, where selected bond angles and distances are reported. The Zn–O bond distances lie within the range 2.03–2.14 Å in agreement with previous findings.[14] The hfac moieties are

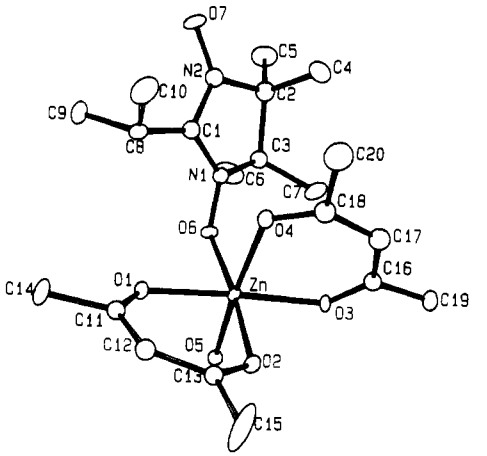

Figure 1. ORTEP view of the asymmetric unit of $Zn(hfac)_2(NITiPr)(H_2O)$. The fluorine atoms were omitted for the sake of clarity.

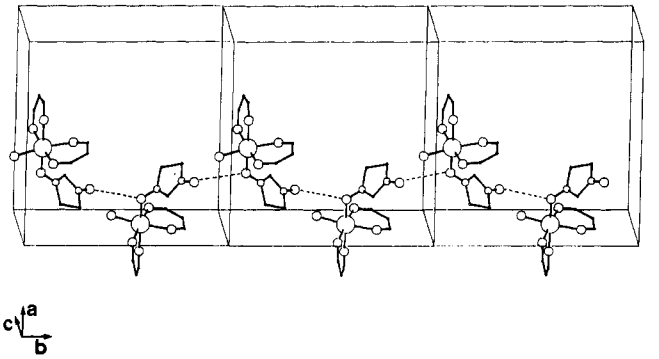

Figure 2. Schematic view of the chain structure of $Zn(hfac)_2(NITiPr)(H_2O)$.

Table III. Selected Bond Distances in Å for $Zn(hfac)_2(NIT_iPr)(H_2O)$[a]

Zn–O1	2.063 (6)	Zn–O2	2.143 (7)
Zn–O3	2.081 (6)	Zn–O4	2.083 (7)
Zn–O5	2.035 (2)	Zn–O6	2.114 (8)
O6–N1	1.308 (11)	O7–N2	1.288 (13)
N1–C1	1.334 (14)	N1–C3	1.477 (14)
N2–C1	1.378 (15)	N2–C2	1.484 (16)
C1–C8	1.451 (17)	C2–C3	1.566 (19)

[a] Standard deviations in the last digit are in parentheses.

Table IV. Selected Bond Angles (deg) for $Zn(hfac)_2(NITiPr)(H_2O)$[a]

O5–Zn–O6	85.6 (3)	O4–Zn–O6	92.0 (3)
O4–Zn–O5	173.0 (3)	O3–Zn–O6	97.3 (3)
O3–Zn–O5	87.1 (3)	O3–Zn–O4	86.8 (3)
O2–Zn–O6	173.8 (3)	O2–Zn–O5	95.2 (3)
O2–Zn–O4	87.9 (3)	O2–Zn–O3	88.9 (3)
O1–Zn–O6	87.8 (3)	O1–Zn–O5	93.6 (3)
O1–Zn–O4	92.7 (3)	O1–Zn–O3	174.8 (3)
O1–Zn–O2	85.9 (3)	Zn–O1–C11	127.3 (7)
Zn–O2–C13	124.0 (7)	Zn–O6–N1	129.6 (6)
O6–N1–C3	119.5 (8)	O6–N1–C1	124.3 (9)
C1–N1–C3	115.3 (9)	O7–N2–C2	123.6 (10)
O7–N2–C1	123.2 (10)	C1–N2–C2	112.9 (9)
N1–C1–N2	106.3 (9)	N1–C1–C8	128.1 (11)
N1–C3–C2	100.3 (9)	N2–C2–C3	101.2 (10)

[a] Standard deviations in the last digit are in parentheses.

(13) Muller, F.; Hopkins, M. A.; Coron, N.; Grynberg, M.; Brunel, L. C.; Martinez, G. *Rev. Sci. Instrum.* **1989**, *60*, 3681. Barra, A. L.; Brunel, L. C.; Robert, J. B. *Chem. Phys. Lett.* **1990**, *165*, 107.

(14) Montgomery, H.; Lingafelter, E. C. *Acta Cryst.* **1963**, *16*, 748.

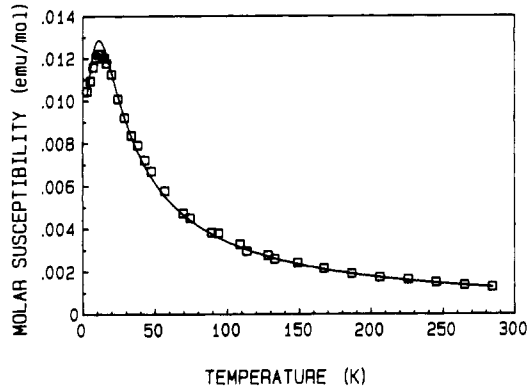

Figure 3. Temperature dependence of the magnetic susceptibility of $Zn(hfac)_2(NITiPr)(H_2O)$. The solid line represents the best fitting values calculated with $J = 12.3$ (5) cm^{-1}.

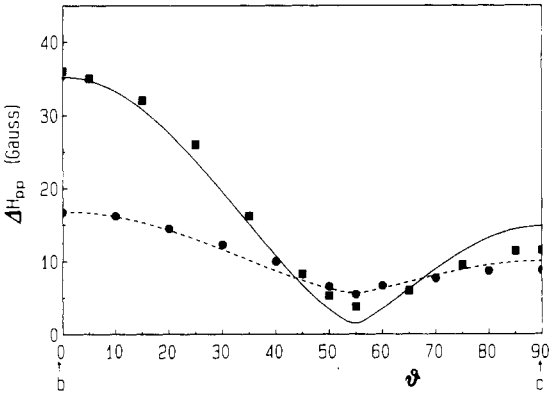

Figure 4. Angular dependence of the EPR line width of $Zn(hfac)_2(NITiPr)(H_2O)$ at room temperature (■) and 4.2 K (●). θ is the angle of the magnetic field with the b axes, and the lines correspond to the best fitting values calculated with the expression $\Delta H_{pp} = a + b(3\cos^2\theta - 1)^{4/3}$.

essentially planar. In the radical the O–N–C–N–O moiety is planar with the other two carbon atoms of the five-membered ring deviating from the plane by ±0.11 Å.

The shortest contact between N–O groups, 3.45 (1) Å, is found between the uncoordinated oxygen atom of the radical, O7, and the coordinated one, O6, of the molecular unit related by the screw axis, as shown in Figure 2, where the content of three unit cells along the b axis is schematically reported. As far as the magnetic interactions are concerned, the relatively short contacts between the NO groups define a chain structure that develops along the b crystallographic axis. From a structural point of view the chain pattern originates in the short contact between the uncoordinated oxygen, O7, of the radical, and the oxygen, O5, of the water molecule, 2.82 (1) Å, which suggests the presence of a hydrogen bond. This interaction keeps the uncoordinated oxygen of the radical close to the metal ion coordination sphere and consequently to the adjacent radical in an unprecedented way.

Magnetic Properties. The room-temperature value of the effective magnetic moment of a powder sample is 1.72 μ_B (χT = 0.369 emu K mol^{-1}), which is a little lower than the value expected for one $S = {}^1/_2$ spin with g equal 2. On decrease of the temperature, the effective magnetic moment decreases steadily and reaches 0.63 μ_B at 5 K. The temperature behavior of the susceptibility is more interesting because it goes through a maximum at about 12 K, as shown in Figure 3.

The polycrystalline powder EPR spectra of $Zn(hfac)_2(NIT$-i-$Pr)(H_2O)$ recorded at X- and Q-band frequency show a single symmetric line at every temperature centered at $g = 2$. A much less intense absorption is observed at half-field ($g = 4$). The X-band spectra of a single crystal show a strong angular dependence of the peak-to-peak line width in the static magnetic field. In Figure 4 we report the results obtained at room temperature and 4.2 K. The line width at room temperature has its maximum (36 G) along the b axis, which corresponds to the chain direction,

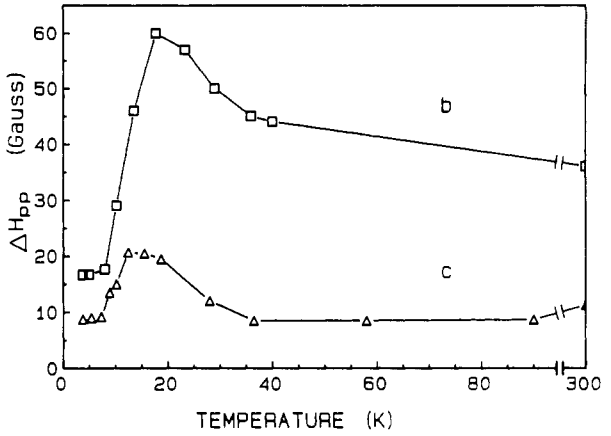

Figure 5. Temperature dependence of the line width of the EPR spectra of $Zn(hfac)_2(NITiPr)(H_2O)$ recorded parallel to the chain direction (b) and perpendicular to it (c).

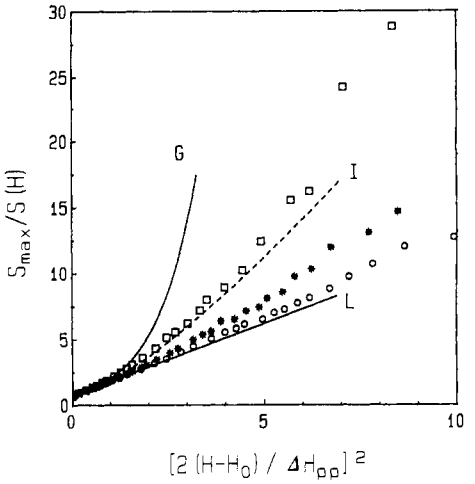

Figure 6. Analysis of the EPR line shape of $Zn(hfac)_2(NITiPr)(H_2O)$: (□) parallel to the chain direction; (*) perpendicular to it; (○) 55° from the chain direction.

goes through a deep minimum (3 G) at about 55° from b, and reaches a second maximum perpendicular to b (11.5 G). In the limit of the accuracy of the experiment, the line width is isotropic in the ac plane, and consequently, we report only one rotation.

The magic angle behavior, which corresponds to a dependence of the line width of the type $(1 - 3\cos^2\theta)^n$, is preserved at low temperature even if the minimum is less pronounced. The values of the extrema are in fact 16.5, 5.5, and 9.0 G along b, at 55°, and perpendicular to b, respectively. The line width presents an anomalous temperature dependence behavior with a well-pronounced maximum of the line width around 20 K in every orientation, as shown in Figure 5.

The analysis of the line shape was performed on the spectra recorded at room and low temperature on a single crystal with the static magnetic field along b, at the magic angle, and perpendicular to b, respectively. The results are plotted in Figure 6 in the form $\{[Y_{max}/Y(H)][(H-H_0)/(H_{max}-H_0)]\}^{1/2}$ vs $[2(H-H_0)/\Delta H_{pp}]$, where Y is the amplitude of the derivative of the absorption. We report also the theoretical value expected for a Gaussian, a Lorentzian, and an intermediate line shape typical of one-dimensional magnetic materials,[15] the last one being the Fourier transform of $\varphi(t) = \exp(-t^{3/2})$. The observed line shape is Lorentzian at the magic angle and intermediate along the chain direction, while in the perpendicular orientation the values are between these two limits. At low temperature the line is Lorentzian in every orientation of the static magnetic field.

Different results are obtained working with a frequency source of 245 GHz, which corresponds to a resonating field of 8.7524

(15) Gatteschi, D.; Sessoli, R. *Magn. Res. Rev.* **1990**, *15*, 1.

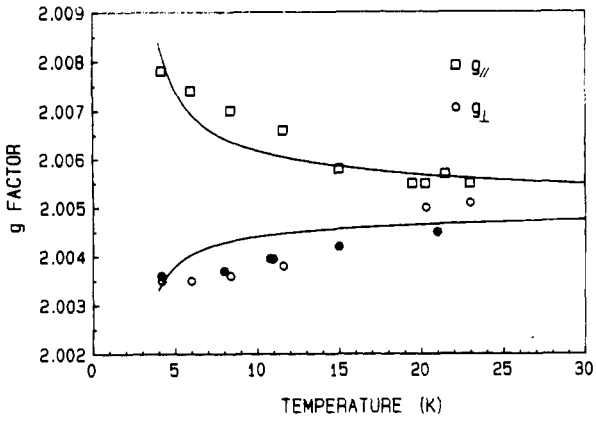

Figure 7. Observed g values of $Zn(hfac)_2(NITiPr)(H_2O)$ at high frequency (245 GHz). The filled symbols refer to the spectra recorded on a single crystal with H perpendicular to b, while the unfilled symbols refer to powder spectra. The solid line represents the calculated values (see text).

T for $g = 2$. In this case the polycrystalline powder spectra recorded at temperatures in the range 4.2–23 K show a pattern typical of axial anisotropy, whose extent increases on lowering the temperature, as shown in Figure 7. We were able to record spectra on a single crystal with the static magnetic field perpendicular to b, and we have observed that the resonance moves to higher fields on lowering the temperature, in agreement with the powder experiments. The line width is larger (34 G) than observed at 9.5 GHz and remains constant without showing any maximum.

Discussion

The crystal structure, the magnetic susceptibility, and the EPR spectra concur to describe $Zn(hfac)_2(NIT\text{-}i\text{-}Pr)(H_2O)$ as a one-dimensional antiferromagnet. Examples of one-dimensional materials made by organic radicals are much rarer than those found by transition-metal ions.[9,16-20] The chains of radicals have in principle very small anisotropy and, they can provide good approximations to one-dimensional Heisenberg antiferromagnets with $S = {}^1/_2$. The temperature dependence of the magnetic susceptibility can be reproduced with the expression valid for Heisenberg $S = {}^1/_2$ chains to yield $J = 12.26$ cm^{-1}, fixing g at 2.00.[21-23] We use the spin Hamiltonian in the form $H = JS_1 \cdot S_2$. The agreement factor defined as $\sum(\chi_{obs} - \chi_{calc})^2/\sum(\chi_{obs})^2$ is $R = 1.7 \times 10^{-3}$. The satisfactory fitting of the χ vs T curve is already a good indication of the one-dimensional nature of $Zn(hfac)_2(NIT\text{-}i\text{-}Pr)(H_2O)$, but it cannot be considered as definitive. Final evidence is provided by the EPR spectra to be discussed below.

The value of the coupling constant can be compared with those previously reported for the interactions between nitronyl nitroxides in systems involving both diamagnetic and paramagnetic metal ions. Exchange-coupling constants ranging from 4 to 135 cm^{-1} were observed.[9,24-26] The origin of the coupling was either direct exchange or superexchange mediated by metal ions.

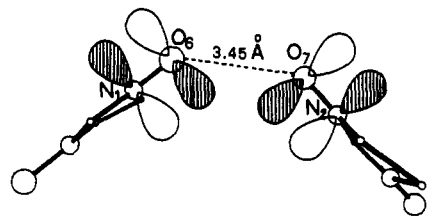

Figure 8. Schematic view of two adjacent radicals and relative magnetic orbitals involved in the interaction.

From the structural point of view the hydrogen bonds with the water molecules determine the one-dimensional nature of the compound, but from the magnetic point of view it is presumably the weak NO–NO interaction that largely determines its one-dimensional antiferromagnetic nature. In fact even if a superexchange pathway passing through the water molecule and the metal ion cannot be ruled out, the presence of direct overlap between the magnetic orbitals of the radicals can largely account for the observed coupling. J compares well with the values previously reported for nitronyl nitroxide compounds where no hydrogen bonding was present and where the NO–NO distances were comparable to that observed here.[24-26]

If we look in detail at the geometry of the contact between two NIT-*i*-Pr molecules, we see that the interacting NO groups are quasi orthogonal to each other (see Figure 8), while in the other cases reported[24-26] so far they were almost parallel to each other. The two NO groups lie approximately on a plane, and the two ONCNO planes of the NIT-*i*-Pr molecules are orthogonal to it and between themselves. With this geometry a small nonzero overlap between the two magnetic orbitals can be anticipated, thus justifying the observed antiferromagnetic coupling.

Although the mechanism of exchange in $Zn(hfac)_2(NIT\text{-}i\text{-}Pr)(H_2O)$ is of the direct type, the observed coupling constant is comparable to those observed in $M(hfac)_3NITR$ one-dimensional materials, M = Y and Eu, where the exchange interaction must be transmitted through the metal ions.[9,16] In $NITpNO_2Ph$ a direct mechanism was assumed to give a ferromagnetic coupling between the radicals.[27]

The analysis of the EPR spectra provides much additional information on the magnetic structure of $Zn(hfac)_2(NIT\text{-}i\text{-}Pr)(H_2O)$. In fact, in one-dimensional antiferromagnets the competition between the dipolar interactions, which tend to give broad Gaussian lines with angular dependence of the type $(3\cos^2\theta - 1)^2$, and the exchange interactions, which tend to give Lorentzian lines with an angular dependence of the type $(1 + \cos^2\theta)$, yields an intermediate situation in which the angular dependence is of the type $(3\cos^2\theta - 1)^{4/3}$, and the line shape is Lorentzian only at the magic angle, while it is intermediate between Gaussian and Lorentzian at the other angular settings.[15,28] The results reported above agree quite well with a one-dimensional description of the magnetic structure of $Zn(hfac)_2(NIT\text{-}i\text{-}Pr)(H_2O)$. The high-temperature spectra are thus typical of a one-dimensional material, confirming that the exchange interaction propagates only within the chains, while the chains are rather well shielded from each other. The fact that the maximum in the line width is observed parallel to the chain axis is in agreement with an essentially dipolar origin of the broadening of the lines. Also, the fact that the curve of the angular dependence of the line width is flatter at low temperature compared to room temperature is understood if one considers that $Zn(hfac)_2(NIT\text{-}i\text{-}Pr)(H_2O)$ is a one-dimensional antiferromagnet. In fact, the typical one-dimensional effects described above are mainly determined by the

(16) Benelli, C.; Caneschi, A.; Gatteschi, D.; Pardi, L.; Rey, P. *Inorg. Chem.* **1989**, *28*, 275.
(17) Lamane, H.; Rey, P.; Rassat, A.; de Comarieu, A.; Michel, J. C. *Mol. Phys.* **1968**, *19*, 201. Kumano, M.; Ikegami, Y. *Chem. Phys. Lett.* **1978**, *54*, 109.
(18) Yamaguchi, J. *Bull. Chem. Soc. Jpn.* **1971**, *33*, 2301.
(19) Endres, H. In *Extended Linear Chain Compounds*; Miller, J. S., Ed.; Plenum Press: New York, 1983; Vol. 3, p 263.
(20) Takahashi, T.; Doi, H.; Nasawa, H. *J. Phys. Soc. Jpn.* **1980**, *48*, 423. Alizon, J.; Berthet, G.; Blanc, J. P.; Gallice, J.; Robert, H.; Thibaud, C. *Phys. Status Solidi B* **1980**, *99*, 363.
(21) Bonner, J. C.; Fisher, M. E. *Phys. Rev.* **1964**, *A135*, 646.
(22) Hall, J. W.; Marsh, W. E.; Weller, R. R.; Hatfield, W. E. *Inorg. Chem.* **1981**, *20*, 1033.
(23) Hatfield, W. E.; Estes, W. E.; Marsh, W. E.; Pickens, M. W.; ter Haar, L. W.; Weller, R. R. In *Extended Linear Chain Compounds*; Miller, J. S., Ed.; Plenum Press: New York, 1983; Vol. 3, p 43.
(24) Caneschi, A.; Gatteschi, D.; Laugier, J.; Rey, P.; Sessoli, R. *Inorg. Chem.* **1988**, *27*, 1553.
(25) Laugier, J.; Rey, P.; Benelli, C.; Gatteschi, D.; Zanchini, C. *J. Am. Chem. Soc.* **1986**, *108*, 6931.
(26) Caneschi, A.; Ferraro, F.; Gatteschi, D.; Rey, P.; Sessoli, R. *Inorg. Chem.* **1990**, *29*, 1756.
(27) Awaga, K.; Inabe, T.; Nagashima, U.; Maruyama, Y. *J. Chem. Soc., Chem. Commun.* **1989**, 1617.
(28) Richards, P. M. In *Local Properties of Phase Transitions*; Editrice Compositori: Bologna, Italy, 1975.

spin modes of long wavelength,[15] i.e. those for which all the spins in the chain are parallel to each other. These modes lose their relevance at low temperature in an antiferromagnet, thus quenching the typical one-dimensional behavior and the magic angle dependence of the line width.

The low-temperature spectra recorded with the high-field EPR spectrometer provide additional useful information on the **g** tensors of the chains, given the high resolution that can be obtained in this case. In fact the spectra recorded at 22 K are quasi-isotropic, but an increasing axial anisotropy shows up on decreasing temperature. The observation of temperature-dependent resonance fields in low-dimensional magnets is well documented.[15,28-31] The origin of this behavior has been attributed to short-range order effects, which build up internal fields that add or subtract to the external magnetic field. In ideal one-dimensional antiferromagnets the resonance shifts downfield parallel to the chain[29-30] and upfield orthogonal to it. Since we experimentally observe that the **g** tensor at 4.2 K is axial with $g_\parallel > g_\perp$, we may reasonably conclude that even at low temperature $Zn(hfac)_2(NIT\text{-}i\text{-}Pr)(H_2O)$ is a well-behaved one-dimensional antiferromagnet.

The quasi-isotropic **g** tensor of $Zn(fhac)_2(NIT\text{-}i\text{-}Pr)(H_2O)$ observed at 22 K must be close to the high-temperature limit, and it agrees with the value expected on the basis of the geometrical arrangement of the NIT-*i*-Pr radicals along the chains. In fact an isolated radical is expected to have a slightly anisotropic **g** tensor, with the principal directions along x, the bisector of the NO directions, z, the direction orthogonal to the ONCNO planes, and y.[32] Although to our knowledge no data have been reported on NITR radicals, the comparison with nitroxides suggest that $g_x \simeq 2.009$, $g_y \simeq 2.006$, and $g_z \simeq 2.003$.[31] The neighboring radicals in the chains are related by the screw axis, and they are oriented in such a way that g_x of one radical is roughly orthogonal to that of the other one, while the g_y directions are parallel to each other. The **g** tensor of the chain must be given by the average of the individual **g** tensors: as a result, a quasi-isotropic $g = 2.006$ is expected, in good agreement with the experimental data at 22 K.

The g shift observed at low temperatures can be calculated with a model taking into account the dipolar anisotropy and the spin correlation length determined by the isotropic exchange-coupling constant in the assumption of a weak Zeeman interaction.[29,30] Using the available formulas, we calculated the temperature dependence of the resonance fields, using the J value calculated for the magnetic susceptibility and using $D = 0.05$ cm^{-1} calculated for two nitronyl nitroxides at a distance of 3.45 Å.[33] The agreement with the experimental data shown in Figure 7 is not very good, but the qualitative behavior is well reproduced. The most obvious flaw of the theoretical treatment is that it assumes small Zeeman interaction, which is certainly not the case in the high-frequency EPR experiment. The temperature dependence of the line width is less well understood. The main feature of X-band spectra is that the line width goes through a maximum at ca. 16 K. This behavior cannot be attributed to a structural phase transition because the high-frequency EPR spectra do not show the same behavior. Further, they confirm that at 4.2 K the system still behaves like a one-dimensional material. Soliton spin wave excitations might be responsible of the observed behavior in low field, while in high fields they might be effectively quenched.[34] A complete characterization using additional exciting frequencies is under way.

Acknowledgment. The financial support of the CNR, of the Progetto Finalizzato "Materiali Speciali per Tecnologie Avanzate", and of MURST is gratefully acknowledged.

Supplementary Material Available: Tables SI–SV, listing experimental and crystallographic parameters, anisotropic thermal factors, positional and thermal parameters of hydrogen atoms, bond distances, and bond angles (6 pages); a table of observed and calculated structure factors (12 pages). Ordering information is given on any current masthead page.

(29) Nagata, K.; Tazuke, Y. *J. Phys. Soc. Jpn.* **1972**, *32*, 337.
(30) Oshima, K.; Okuda, K.; Date, M. *J. Phys. Soc. Jpn.* **1977**, *43*, 1131.
(31) Caneschi, A.; Gatteschi, D.; Renard, J.-P.; Rey, P.; Sessoli, R. *Inorg. Chem.* **1989**, *28*, 3314. Gatteschi, D.; Guillou, O.; Zanchini, C.; Sessoli, R.; Kahn, O.; Verdaguer, M.; Pei, Y. *Inorg. Chem.* **1989**, *28*, 297.
(32) Berliner, L. J. *Spin Labeling*; Academic Press: New York, 1976; p 565.
(33) The magnetic dipolar interaction was calculated with the point dipolar approximation dividing the energy by a factor 2 in order to take into account that the unpaired electron is delocalized on the two NO groups.
(34) de Jong, L. J. In *Magneto-Structural Correlations in Exchange Coupled Systems*; Willett, R. D., Gatteschi, D., Kahn, O., Eds.; Reidel: Dordrecht, The Netherlands, 1985; p 1. Thiel, R. C.; de Graaf, H.; de Jongh, L. J. *Phys. Rev. Lett.* **1981**, *47*, 1415.